IMF-driven overshielding electric field and the origin of the plasmaspheric shoulder of May 24, 2000

J. Goldstein,[1] R. W. Spiro,[1] P. H. Reiff,[1] R. A. Wolf,[1] B. R. Sandel,[2]
J. W. Freeman,[1] and R. L. Lambour[3]

Received 7 December 2001; revised 3 April 2002; accepted 9 April 2002; published 31 August 2002.

[1] Between the hours of 6–10 UT on May 24, 2000, the IMAGE extreme ultraviolet (EUV) instrument observed a shoulder-shaped bulge in the morning sector plasmapause [*Burch et al.*, 2001a, 2001b]. Simulation results of the data-driven Magnetospheric Specification Model (MSM) have reproduced the formation (during 4:00–5:15 UT) and subsequent evolution of the shoulder. In the model, the shoulder is created by a dusk-to-dawn overshielding electric field, triggered by two sudden, strong northward (N_{wd}) turnings of the IMF. Overshielding causes antisunward flow of predawn plasma, producing an asymmetric bulge that rotates eastward. *INDEX TERMS:* 2730 Magnetospheric Physics: Magnetosphere—inner; 2740 Magnetospheric Physics: Magnetospheric configuration and dynamics; 2760 Magnetospheric Physics: Plasma convection; 2712 Magnetospheric Physics: Electric fields (2411); 2768 Magnetospheric Physics: Plasmasphere

1. Introduction

[2] The plasmapause results primarily from a superposition of corotation and convection electric (E) fields in the inner magnetosphere [*Nishida*, 1966; *Kavanagh et al.*, 1968], although it is not known in detail how a new plasmapause forms, especially during active times. Irregular plasmapause features such as 'bite-outs' and 'tails' occur often in both whistler and in situ data [*Carpenter et al.*, 1993; *Moldwin et al.*, 1994; *Carpenter and Lemaire*, 1997].

[3] Alongside observations, simulations have offered a larger picture of the plasmasphere, unavailable in previous in situ and ground-based measurements. This letter presents calculations of the Magnetospheric Specification Model (MSM), a data-driven model of global magnetospheric convection [*Freeman et al.*, 1993; *Wolf et al.*, 1997; *Weiss et al.*, 1997; *Lambour et al.*, 1997]. The version of MSM used in this study deals only with the cold (.001 eV) plasma, and contains a simple plasmaspheric module with refilling [*Lambour et al.*, 1997]. The initial conditions (ICs) are set by specifying the plasmapause boundary, and allowing the electron density inside that boundary to follow the saturated model of *Carpenter and Anderson* [1992]. The MSM's convection E-field is a parametric model based on characteristic results from the Rice Convection Model (RCM). It is both spatially nonuniform and dynamically responsive to changing geomagnetic and solar wind conditions, in agreement with modeling results of *Spiro et al.* [1988] and observational work by *Fejer et al.* [1990]. To drive the MSM, several inputs are used: K_p; D_{st}; solar wind (SW) and interplanetary magnetic field (IMF) data; ABI, the auroral boundary index of *Gussenhoven et al.* [1983]; PCP, the cross-polar cap potential. SW and IMF conditions can be measured by the ACE, Wind, IMP-8, and/or Geotail spacecraft. The PCP is either inferred from DMSP measurements (if available), or SW and IMF data are used in the empirical formula of *Boyle et al.* [1997] to calculate PCP_B.

[4] With the launch of the IMAGE satellite in March, 2000, a new era of global observation of the plasmasphere began. The extreme ultraviolet imager (EUV) on IMAGE is a three-camera system that detects 30.4 nm radiation emitted by He^+ ions [*Sandel et al.*, 2000]. EUV provides, for the first time, routine global images of the helium plasmasphere, thus offering the same global view available via simulation. EUV images verify that the plasmapause is seldom smooth or regular, in agreement with whistler and in situ observations. 'Tails,' 'plasma voids,' 'fingers,' 'bite-outs,' and 'shoulders' are some of the features seen by EUV [*Sandel et al.*, 2001]. While it is believable that tails are due to 'drainage' of plasmaspheric material by convection [*Grebowsky*, 1970; *Chen et al.*, 1975], convincing explanations for the other features have yet to be found. One of these unexplained features, the shoulder, may act as a loss mechanism for the ring current [*Burch et al.*, 2001a]. This letter proposes a hypothetical explanation, arising from MSM simulation output, for the formation of the plasmaspheric shoulder of May 24, 2000 [*Burch et al.*, 2001a, 2001b].

2. EUV Observation of May 24 Shoulder

[5] On May 24, 2000, IMAGE's trajectory was as depicted in the 3D orbit plot, in SM coordinates, of the right panel of Figure 1. Each orbit, EUV data was acquired while IMAGE was close to apogee, looking down upon the north pole of the Earth. From 6:03 UT–10:14 UT (designated interval 'B'), as IMAGE rose up from the dusk side, EUV observed a shoulder-like bulge in the morning sector plasmapause. Asymmetric in magnetic local time (MLT), the shoulder had a sharp eastern edge about 0.5 R_E in radial extent that gradually tapered off on the west side. There are no observations of the formation of the shoulder; the preceding interval of EUV data (16:43–18:43 UT on May 23, interval 'A') did not include a shoulder.

[6] Figure 1 (left panel) is an EUV snapshot from 7:04 UT, taken from a vantage point indicated in the orbit plot, about one hour after the first observation of the shoulder at

[1]Department of Physics and Astronomy, Rice University, Houston, Texas, USA.
[2]Lunar and Planetary Laboratory, University of Arizona, Tucson, Arizona, USA.
[3]Lexington, Massachusetts, USA.

0094-8276/02/2001GL014534$05.00

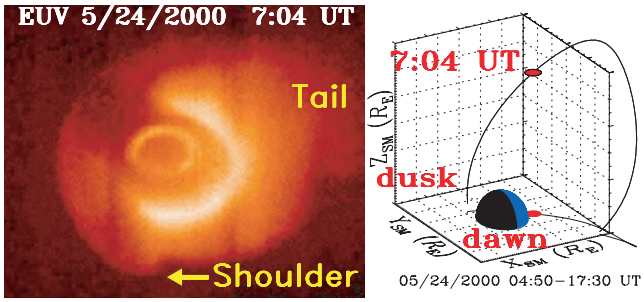

Figure 1. Snapshot of plasmasphere (left panel) by EUV imager, 7:04 UT, from vantage point indicated in orbit plot (right panel). Sunlight is incident from the lower right; Earth is in the center. The bright inner ring is the auroral oval. The shoulder is in the morning MLT, and a drainage tail is in the afternoon sector.

the start of interval B. The plasmapause is assumed to be the sharp edge where the brightness of 30.4 nm He^+ emissions drops drastically. The shoulder (labeled, and marked by the arrow) presumably formed in the pre-dawn sector in the time between intervals A and B. Subsequent EUV images [*Burch et al.*, 2001b] show the shoulder rotating eastward, sharpening in MLT as it goes. By 'sharpening in MLT' it is meant that the outer edge of the shoulder (i.e., the edge that is further out in radius) rotates faster than the inner edge, resulting in a gradually increasing steepness in the MLT-profile of the shoulder. This sharpening is not merely a by product of perspective. Evident in the afternoon region is a drainage tail (labeled, 'Tail'). At first, the MLT extent of the tail was from noon to dusk (see Figure 1); over the next few hours, the western edge of the tail moved eastward from its noon position, so that the tail 'thinned out' (see the EUV image sequence of *Burch et al.* [2001b]). The next section discusses simulation of the May 24 shoulder and tail.

3. MSM Simulation

[7] For May 24, 2000, all of the MSM inputs were available or derivable. Solar wind (SW) and IMF data were measured by the Wind spacecraft, and delayed by 7.5 minutes to account for the propagation time, at the measured SW velocity of 600 km s^{-1}, from Wind's location 42 R_E upstream. Due to sparseness of DMSP data, PCP_B was used for much of the simulation run. On May 23–24, the average deviation of PCP_B from available PCP was about 18 percent.

[8] As ICs for the MSM, the EUV-observed plasmapause at the start of interval A was modeled by an 8-term Fourier series: $L_{pp} = A_0 + \frac{1}{10}\sum_{n=1}^{4}[b_n \sin(nx) - a_n \cos(nx)]$, where $\boldsymbol{a}$ = [1, 3, 1, 4] and $\boldsymbol{b}$ = [0, 1, 3, 1]. (Note that an independent run, with a circular plasmapause at $L_{pp} = 3.5$, yielded output visually identical to that of the run with the ICs stated above. Evidently, the MSM results do not strongly depend on azimuthal structure in the plasmapause ICs.) The MSM was run with 15-minute time resolution from May 23, 16:00 UT, until May 24, 10:15 UT. Thus, the simulation spanned both intervals A and B, and all times in between. A snapshot of MSM output at 7 UT is shown in Figure 2, a plot of the equatorial electron density in SM coordinates. We identify MSM's plasmapause as the sharpest density gradient, at the border between yellow and red, at about 150 cm^{-3}. Comparing Figures 1 and 2, both the shoulder and tail of the 7:04 UT EUV image are evident in the 7 UT MSM snapshot. The model's time development compares favorably as well. The MSM tail 'thinned' in MLT, as in EUV images. Both the EUV and MSM shoulders moved eastward during 6–9 UT, sharpening in MLT as they went. Figure 3 plots the rotation through MLT of the eastward edge of the shoulder, according to EUV (dashed line) and MSM (solid). Their rates slightly exceed strict corotation: MSM by 8% and EUV by 1%.

[9] The overall agreement between MSM and EUV is quite good, but three details differ. (1) The MSM shoulder is blurrier, less distinct. (2) From Figure 3, the MSM shoulder is located ~1.5 hr. earlier in MLT. (3) The MSM tail densities seem lower, relative to the bulk of the plasmasphere. (1) and (3) are possibly due to numerical diffusion. (2) can be attributed to the statistical origin of the MSM E-field model (see section 4).

[10] Although unobserved by EUV, formation of the shoulder was captured by MSM, and took place in the pre-dawn region. The shoulder's creation was manifested as an outward radial motion of plasma in a narrow range of MLT (roughly 3–5 MLT). At timestep T_n, there is 'shoulder growth' (SG) if the shoulder's outer edge is further out in radius than at the previous step T_{n-1}. Thus defined, SG ensued during 4–4:15 UT (2 timesteps) and 4:45–5:15 (3 timesteps). Examining both IMF data and MSM-calcuated electric potential, it is possible to explain shoulder formation as due to penetration E-field, as follows.

3.1. Penetration Electric Field

[11] Electric fields form at the Earthward edge of the plasmasheet to counteract the effects of SW/IMF-driven

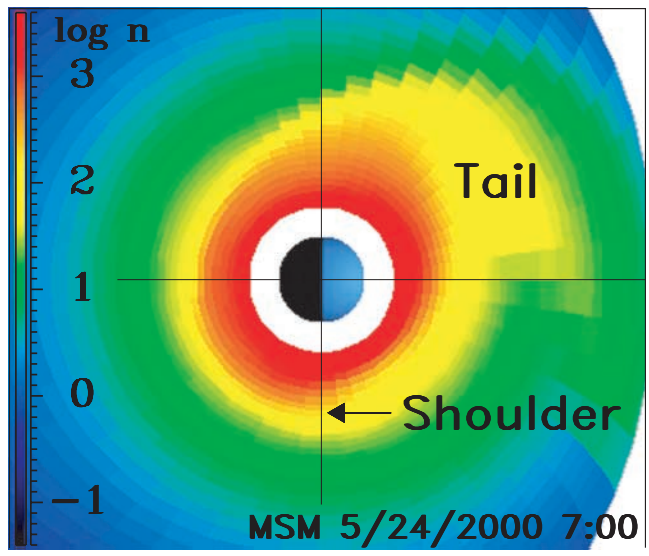

Figure 2. Snapshot of MSM simulated plasmasphere with shoulder and tail, 7 UT on May 24, roughly to scale with Figure 1. The sun is to the right. The white circle around Earth marks the inner simulation boundary, ~1.7R_E. Colors depict $\log_{10}$ scaled electron density n [cm^{-3}] (see legend).

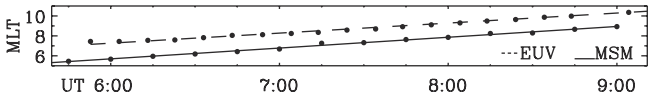

Figure 3. MLT of eastward edge of shoulder, EUV and MSM. (Dot = extracted position. Line = linear fit.)

convection, thus 'shielding' the inner magnetosphere (IM) from externally imposed E-fields [e.g., *Jaggi and Wolf*, 1973]. However, if the SW/IMF conditions change faster than the shielding timescale τ_s (where $\tau_s \leq 1$ hour [*Kelley et al.*, 1979]), there can be significant E-fields in the IM; such fields are here designated 'penetration E-fields,' and take two forms. If convection grows faster than τ_s, 'under-shielding' occurs, and a dawn-to-dusk convection E-field (with concomitant sunward plasma flow) is imposed upon the IM until the shielding layer adjusts to the new conditions. On the other hand, 'overshielding' arises if a residual dusk-to-dawn shielding E-field (i.e., antisunward flow) remains after a sudden decrease in the strength of magnetospheric convection, such as might ensue after a sudden northward (N_{wd}) turning of the IMF B_Z component [*Kelley et al.*, 1979].

[12] Two such sudden N_{wd} turnings of the IMF did occur during the May 24 storm (minimum $D_{st} = -150$ nT; maximum $K_p = 8$), on the heels of over two hours of southward (S_{wd}) IMF, ~600 km s^{-1} SW speed, and 30–40 cm^{-3} SW density. The N_{wd} turnings were at about 3:45 UT and 4:40 UT, as shown in Figure 4, a plot of the propagation-delayed Wind IMF data. Following *Burch et al.* [2001a], we can extrapolate the shoulder back to the time of these N_{wd} turnings by moving backward in local time, assuming strict corotation. This local time extrapolation puts the EUV-observed shoulder in the pre-dawn sector at the time of the N_{wd} turnings, where and when the shoulder formed in the MSM simulation. The intervals of MSM shoulder growth (SG) are overlaid on Figure 4 as shaded boxes; SG follows in response to the N_{wd} turnings. The connection between the IMF transitions and SG is the overshielding (penetration) E-field, which is accompanied by outward plasma flow in a narrow MLT sector.

[13] Figure 5a shows a snapshot (at 5 UT, shortly after the second IMF turning) of the MSM electric potential Φ_{MSM} imposed upon the IM, ignoring corotation. Colors give Φ_{MSM} in kV; black equipotential contour lines are also flowlines. The arrows indicate the directions (but not the magnitudes) of the imposed IM flow pattern. E-fields point from high potential (yellow) to low (blue). There is a dawn-to-dusk convection E-field in the outer magnetosphere, imposing a flow that is globally sunward (to the right). In the IM, overshielding creates an E-field that points from dusk to dawn, imposing an antisunward (to the left) flow. The net imposed field is nonuniform and nonaxisymmetric, and tries to create a counter-clockwise (CCW) 'eddy' flow near dawn (see arrows circling blue contours), and a weaker clockwise (CW) eddy near dusk. These eddy flows arise due to the conjunction of oppositely-directed flows at the boundary between the inner and outer magnetosphere. The strongest antisunward flow (where the flowlines are closest together) occurs in the pre-dawn sector, inside the red oval henceforth called the 'active' region ('AR'). The AR occurs in the narrow MLT region where the dawnside and duskside eddy flows both point antisunward; in this MLT range, the antisunward direction is also radial. Thus, in the AR, imposed flow is radially outward.

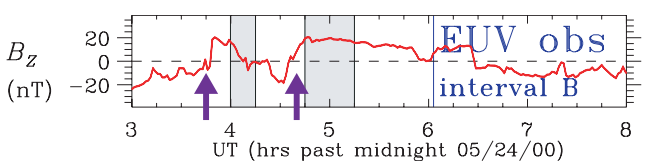

Figure 4. Propagation-delayed May 24 Wind IMF B_Z. Two sudden northward turnings (arrows) are at ~3:45 and ~4:40 UT, preceding interval B.

[14] The effect of the imposed field is found by adding it to the corotation potential (or flow) field; this is shown in Figure 5b. Colors are log number density (the plasmasphere is red/orange). Overlayed on the density colors are black contour lines that show total IM potential due to both convection and corotation: $\Phi = \Phi_{MSM} + \Phi_{cor}$. The arrows are flow vectors; only flow speeds above $1.2 \times 10^{-4} R_E/s$, and inside the plasmasphere, are shown. Corotational flow is eastward, along flowlines that are (approximately) geocentric circles. This eastward corotation flow is slightly augmented near dusk by the weak eastward eddy flow imposed there (shown in Figure 5a). In contrast, at the dawn terminator, the imposed CCW eddy flow opposes plasmaspheric corotation, causing a pseudo-stagnation point (labeled 'S') where flows are very weak. West of 'S' is the AR, where the imposed flow contributes to corotation, producing a net outward/eastward flow as shown in Figure 5b. It is in the AR that the bulk plasma motion is most pronounced, and therefore where the plasmapause 'bulges out' most, forming the shoulder. This already strong AR bulge is accentuated on the eastward side by the lack of strong flows at S; this explains the asymmetry of the shoulder. The MLT profile of the magnitude of AR flow nicely echoes the observed shoulder shape. The maximum flow speed in the AR is about $2 \times 10^{-4} R_E/s$; multiplied by 45 min of total overshielding time, this gives shoulder radial size 0.5 R_E, in agreement with EUV. Successive N_{wd} jumps on May 24 did not create two distinct shoulders because the AR is broader in MLT than the angle the shoulder rotates through, between jumps. The IMF swings S_{wd} again after 6:30 (Figure 4), and

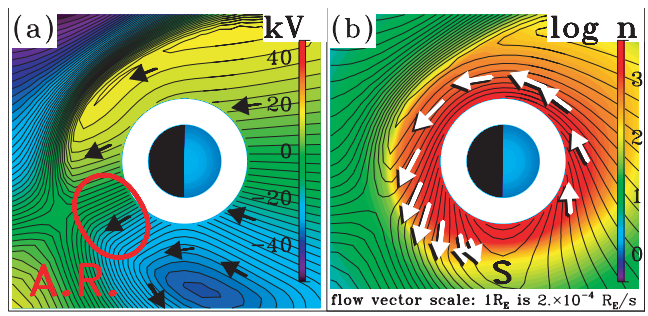

Figure 5. Two panels of MSM output, 5 UT. (a) Contours of potential Φ_{MSM}. The shoulder formed in the pre-dawn active region ('A.R.', red oval). (b) Black contours Φ and vectors show actual flow, including corotation. Color is log electron density.

is unsteady, causing weak (and intermittent) undershielding. Shear in the eastward component of the penetration velocity field causes the outer part of the shoulder to rotate faster. This is why the shoulder sharpens in MLT, and why its average rotation rate exceeds strict corotation.

4. Discussion

[15] The pattern of the MSM's penetration E-field was designed to match RCM simulations [*Spiro et al.*, 1988], which agree with the statistical pattern derived from Jicamarca radar data. The basic pattern, and particularly the concentration of azimuthal E-field in the AR, was derived independently by *Senior and Blanc* [1984], and confirmed by ground radar [*Fejer and Scherliess*, 1995]. Other observations fit our overshielding interpretation: eastward E-fields observed in the equatorial ionosphere in response to N_{wd} turnings of the IMF [*Kelley et al.*, 1979]; and rapid outward drift of post-midnight plasma seen in whistler data (and inferred from Geotail wave data) in the aftermath of isolated substorms [*Carpenter and Smith*, 2001].

[16] We have demonstrated that the May 24, 2000 shoulder seems to be associated with nonuniform, nonaxisymmetric overshielding. Shoulders have been identified in over a dozen events. (Three of these events are discussed by *Burch et al.* [2001a]). Preliminary simulation results indicate that these shoulders can also be linked to N_{wd} IMF turnings. It is likely that shoulders form in other situations as well. During storms, fast inward drifts occurring preferentially in post-midnight MLT [*Carpenter and Lemaire*, 1997] may create a large 'bite-out;' i.e., a wedge of MLT where plasmapause radius is reduced. If bite-out formation is followed by sudden quieting, one edge of the bite-out could evolve into a shoulder. Storm-time undershielding might push dayside plasma sunward, creating a bulge [*Lemaire*, 2000]. Shoulder effects might also develop when drainage tails rotate through nightside during quieting. The hypothetical connection between N_{wd} IMF turnings and shoulders requires further testing, to be reported in future papers already underway.

[17] **Acknowledgments.** We are grateful for data provided by F. Rich of AFRL (ABI), M. Hairston of U.T. Dallas (PCP), the Kyoto WDC-C2 web site (D_{st}), the National Geophysical Data Center web site (K_p), and the NSSDC OMNI-Web site (SW/IMF). We acknowledge D. Carpenter for useful discussions. The authors would like to thank the referees, and the editor, for their careful review of this paper. Work at Rice was supported by NASA contract NAS5-96020 with SwRI, and in part by NASA SEC Theory grant NAG5-8136 and NSF-ATM-9802744. Work at U. Arizona funded by Contract 83818 from SwRI, a subcontract under NASA NAS5-96020.

References

Boyle, C. B., P. H. Reiff, and M. R. Hairston, Empirical polar cap potentials, *J. Geophys. Res.*, *102*, 111, 1997.

Burch, J. L., D. G. Mitchell, B. R. Sandel, P. C. Brandt, and M. Wüest, Global dynamics of the plasmasphere and ring current during magnetic storms, *Geophys. Res. Lett.*, *28*, 1159, 2001a.

Burch, J. L., et al., Views of Earth's magnetosphere with the IMAGE satellite, *Science*, *291*, 619, 2001b.

Carpenter, D. L., and R. R. Anderson, An ISEE/Whistler model of equatorial electron density in the magnetosphere, *J. Geophys. Res.*, *97*, 1097, 1992.

Carpenter, D. L., and J. Lemaire, Erosion and recovery of the plasmasphere in the plasmapause region, *Space Sci. Rev.*, *80*, 153, 1997.

Carpenter, D. L., and A. J. Smith, The study of bulk plasma motions and associated electric fields in the plasmasphere by means of whistler-mode signals, *J. Atmos. Solar-Terr. Phys.*, *63*, 1117, 2001.

Carpenter, D. L., B. L. Giles, C. R. Chappell, P. M. E. Decreau, R. R. Anderson, A. M. Persoon, A. J. Smith, Y. Corcuff, and P. Canu, Plasmasphere dynamics in the dusk-side bulge region: a new look at an old topic, *J. Geophys. Res.*, *98*, 19,243, 1993.

Chen, A. J., J. M. Grebowsky, and H. A. Taylor Jr., Dynamics of midlatitude light ion trough and plasma tails, *J. Geophys. Res.*, *80*, 968, 1975.

Fejer, B. G., and L. Scherliess, Time dependent response of equatorial ionospheric electric fields in magnetospheric disturbances, *Geophys. Res. Lett.*, *22*, 851, 1995.

Fejer, B. G., R. W. Spiro, R. A. Wolf, and J. C. Foster, Latitudinal variation of perturbation electric fields during magnetically disturbed periods: 1986 SUNDIAL observations and model results, *Ann. Geophys.*, *8*, 441, 1990.

Freeman, J. W., et al., Magnetospheric Specification Model development code and documentation. Report for USAF contract F19,628-90-K-0012, Rice University, Houston, TX, 1993.

Grebowsky, J. M., Model study of plasmapause motion, *J. Geophys. Res.*, *75*, 4329, 1970.

Gussenhoven, M. S., D. A. Hardy, and N. Heinemann, Systematics of the equatorward diffuse auroral boundary, *J. Geophys. Res.*, *88*, 5692, 1983.

Jaggi, R. K., and R. A. Wolf, Self-consistent calculation of the motion of a sheet of ions in the magnetosphere, *J. Geophys. Res.*, *78*, 2852, 1973.

Kavanagh, L. D., J. W. Freeman Jr., and A. J. Chen, Plasma flow in the magnetosphere, *J. Geophys. Res.*, *73*, 5511, 1968.

Kelley, M. C., B. G. Fejer, and C. A. Gonzales, An explanation for anomalous ionospheric electric fields associated with a northward turning of the interplanetary magnetic field, *Geophys. Res. Lett.*, *6*, 301, 1979.

Lambour, R. L., L. A. Weiss, R. C. Elphic, and M. F. Thomsen, Global modeling of the plasmasphere following storm sudden commencements, *J. Geophys. Res.*, *102*, 24,351, 1997.

Lemaire, J., The formation of plasmaspheric tails, *Phys. Chem. Earth (C)*, *25*, 9, 2000.

Moldwin, M. B., et al., An examination of structure and dynamics of the outer plasmasphere using multiple geosynchronous satellites, *J. Geophys. Res.*, *99*, 11,475, 1994.

Nishida, A., Formation of plasmapause, or magnetospheric plasma knee, by the combined action of magnetospheric convection and plasma escape from the tail, *J. Geophys. Res.*, *71*, 5669, 1966.

Sandel, B. R., R. A. King, W. T. Forrester, D. L. Gallagher, A. L. Broadfoot, and C. C. Curtis, Initial results from the IMAGE extreme ultraviolet imager, *Geophys. Res. Lett.*, *28*, 1439, 2001.

Sandel, B. R., et al., The extreme ultraviolet imager investigation for the IMAGE mission, *Space Sci. Rev.*, *91*, 197, 2000.

Senior, C., and M. Blanc, On the control of magnetospheric convection by the spatial distribution of ionospheric conductivities, *J. Geophys. Res.*, *89*, 261, 1984.

Spiro, R. W., R. A. Wolf, and B. G. Fejer, Penetration of high-latitude-electric-field effects to low latitudes during SUNDIAL 1984, *Ann. Geophys.*, *6*, 39, 1988.

Weiss, L. A., R. L. Lambour, R. C. Elphic, and M. F. Thomsen, Study of plasmaspheric evolution using geosynchronous observations and global modeling, *Geophys. Res. Lett.*, *24*, 599, 1997.

Wolf, R. A., et al., Modeling convection effects in magnetic storms, in *Magnetic Storms*, edited by B. T. Tsurutani, p. 161, AGU, Washington, D. C., 1997.

J. Goldstein, R. W. Spiro, P. H. Reiff, R. A. Wolf, and J. W. Freeman, Dept of Physics and Astron, Rice Univ, Houston, TX 77005, USA. (jerru@rice.edu)

B. R. Sandel, Lunar and Planetary Laboratory, University of Arizona, Tucson, AZ 85721, USA.

R. L. Lambour, 244 Wood Street, Lexington, MA 02420, USA.